nature portfolio

https://doi.org/10.1038/s41557-021-00701-6

Supplementary information

Dinitrogen binding and activation at a molybdenum–iron–sulfur cluster

In the format provided by the authors and unedited

Supplementary Information for:

Dinitrogen Binding and Activation at a Molybdenum–Iron–Sulfur Cluster

*Alex McSkimming and Daniel L. M. Suess**

Department of Chemistry, Massachusetts Institute of Technology, Cambridge, MA 02139

Contents

Supplementary Data and Discussion

NMR Spectroscopy

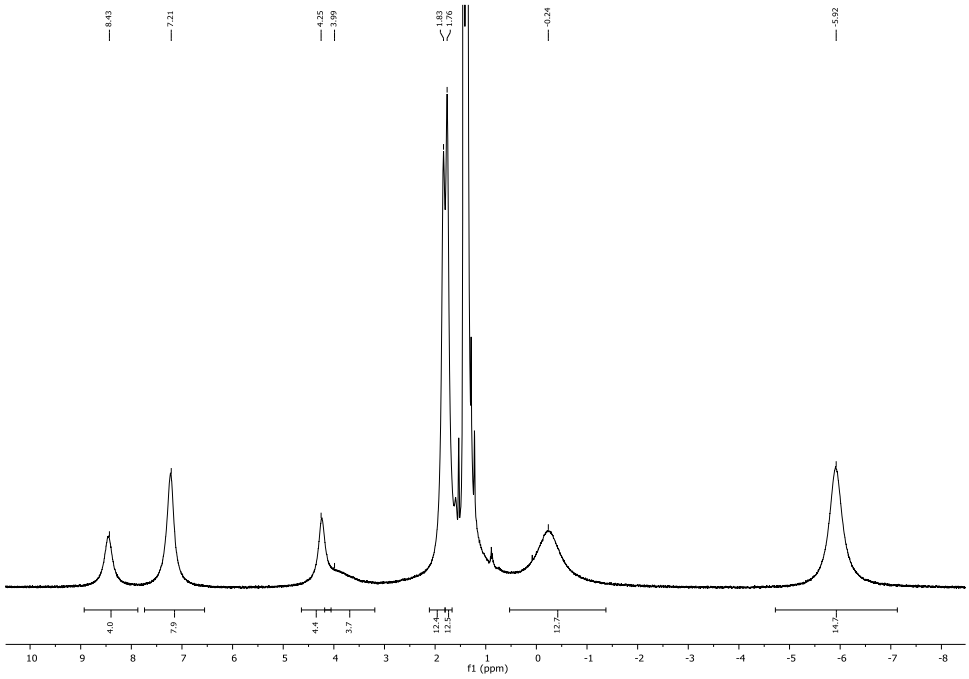

Supplementary Figure 1. ^{1}H NMR spectrum of **1** in *cyc*-C_6D_{12} recorded at 400 MHz.

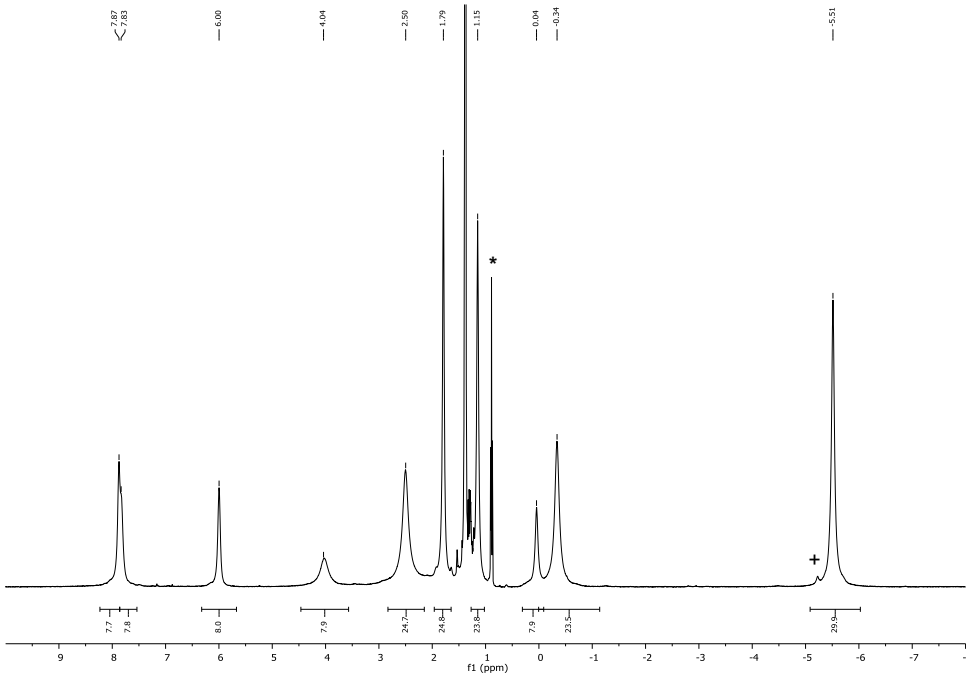

Supplementary Figure 2. ^{1}H NMR spectrum of **2** in *cyc*-C_6D_{12} recorded at 400 MHz. ***** *n*-Pentane solvent of crystallization; **+** Cp***** resonance of a small impurity, possibly a result of thermal decomposition.

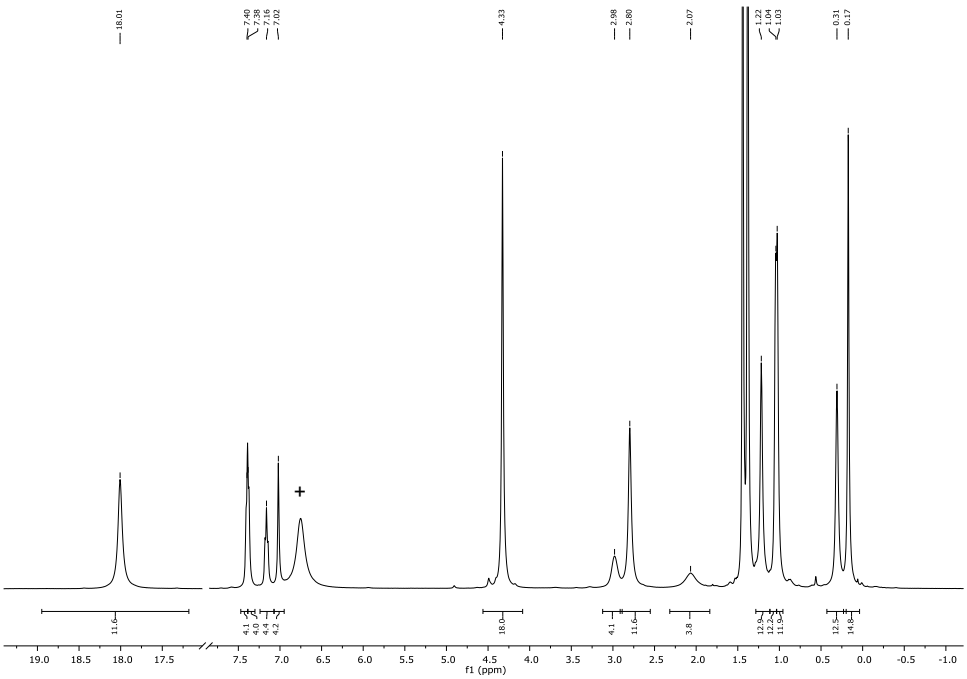

Supplementary Figure 3. ^{1}H NMR spectrum of **3** in the presence of 1 equiv. $(C_5(Me)_4SiMe_3)_2Ti$ in *cyc*-C_6D_{12} recorded at 400 MHz. **+** resonance due to $(C_5(Me)_4SiMe_3)Ti$.

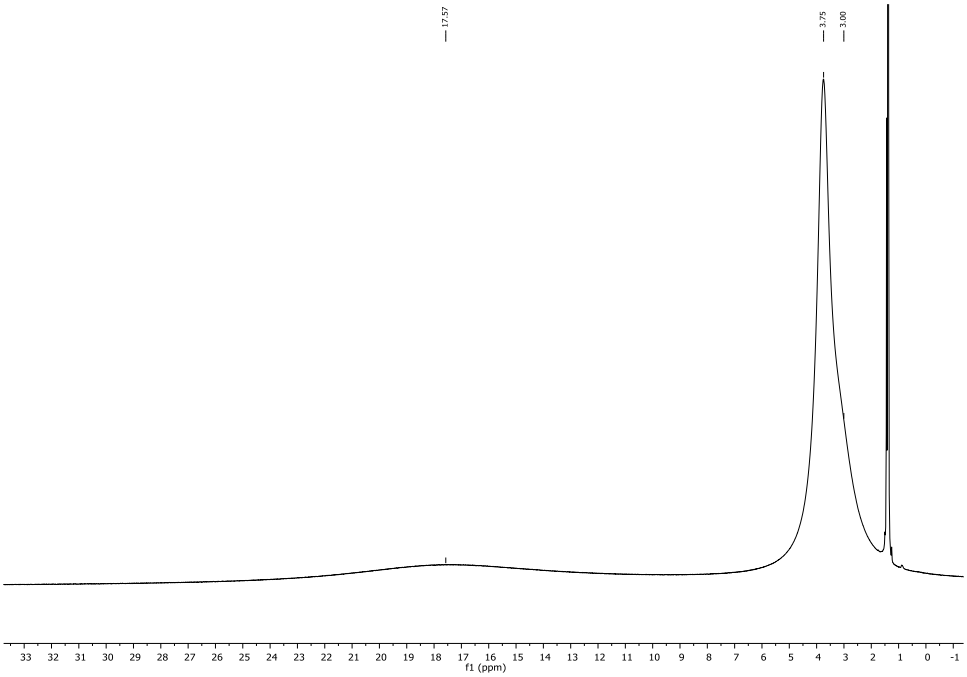

Supplementary Figure 4. ^{1}H NMR spectrum of $(C_5(Me)_4SiMe_3)_2TiCl$ in *cyc*-C_6D_{12} recorded at 400 MHz. The two upfield signals have been de-convoluted using peak fitting software. Chemical shifts are as follows: δ 17.57, 3.75, 3.00.

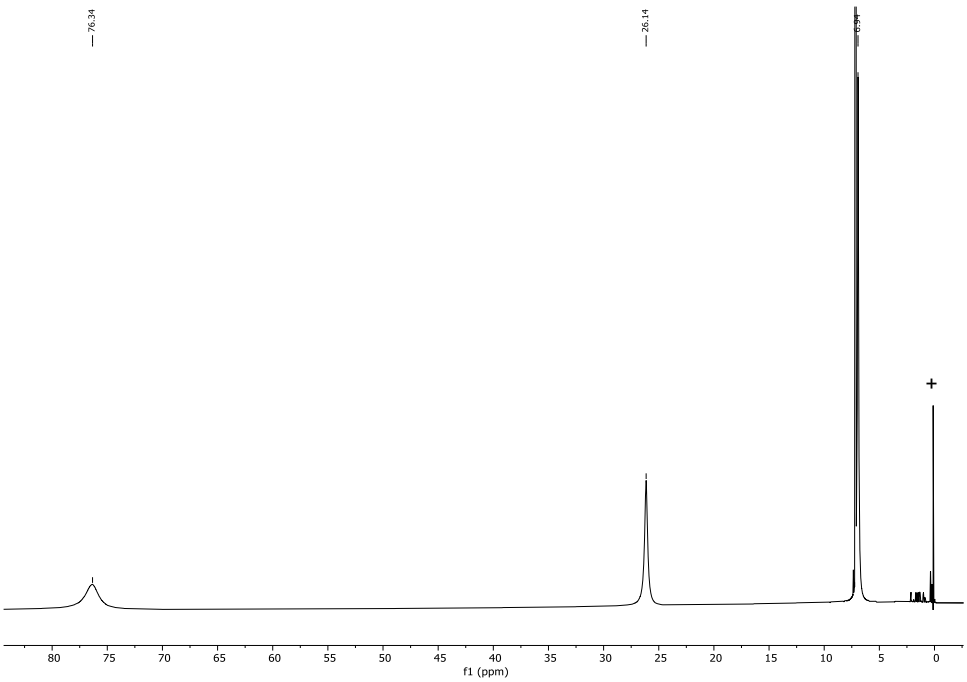

Supplementary Figure 5. ^{1}H NMR spectrum of $(C_5(Me)_4SiMe_3)_2Ti$ in C_6D_6 recorded at 400 MHz. **+** resonance due to trace $[(CH_3)_3Si]_2O$ (re-crystallization solvent). Chemical shifts are as follows: δ 76.34, 26.14, 6.94 ppm.

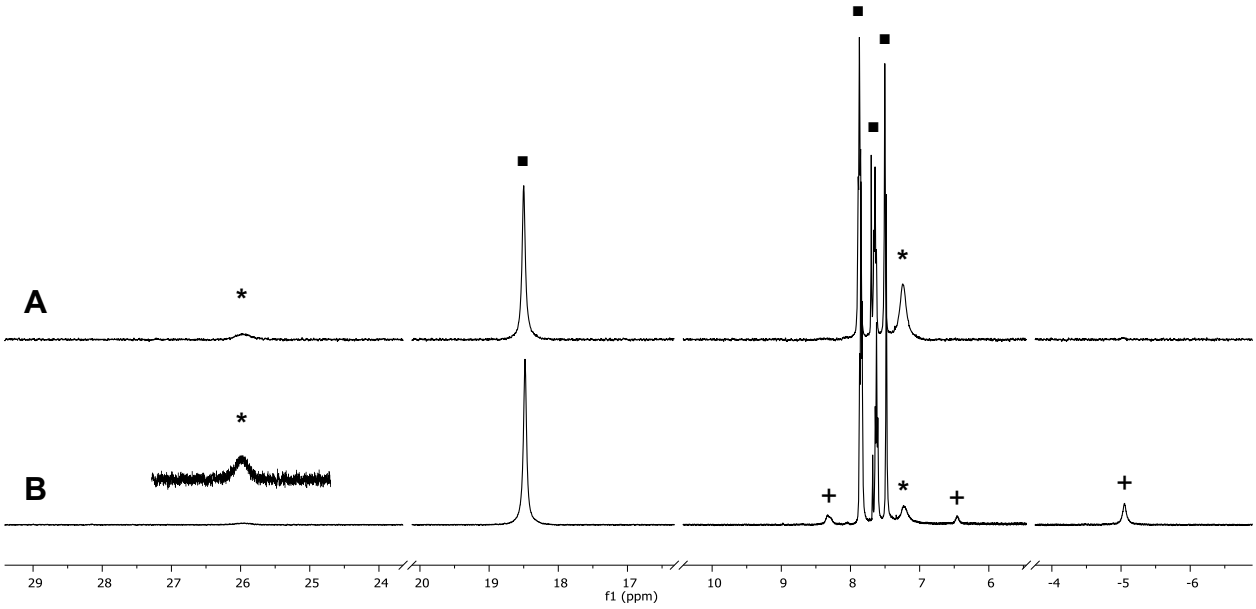

Supplementary Figure 6. ^{1}H NMR spectra recorded in *cyc*-C_6H_{12} (solvent suppressed) of (A) a mixture of **2** and 3 equiv $(C_5(Me)_4SiMe_3)_2Ti$ and (B) crystalline **3** obtained from this mixture as described in the Methods section, showing the generation of **2**. Upon addition of a further equivalent of $(C_5(Me)_4SiMe_3)_2Ti$ to (B), peaks for **2** ablate and spectrum A is re-obtained. Taken together, these findings suggest that **2**, **3**, and $(C_5(Me)_4SiMe_3)_2Ti$ are in equilibrium under an N_2 atmosphere. Peaks are labelled as follows: * $(C_5(Me)_4SiMe_3)_2Ti$; **+ 2**; ■ **3**. Inset is a blow-up of the resonance at δ 26.

FT-IR Spectroscopy

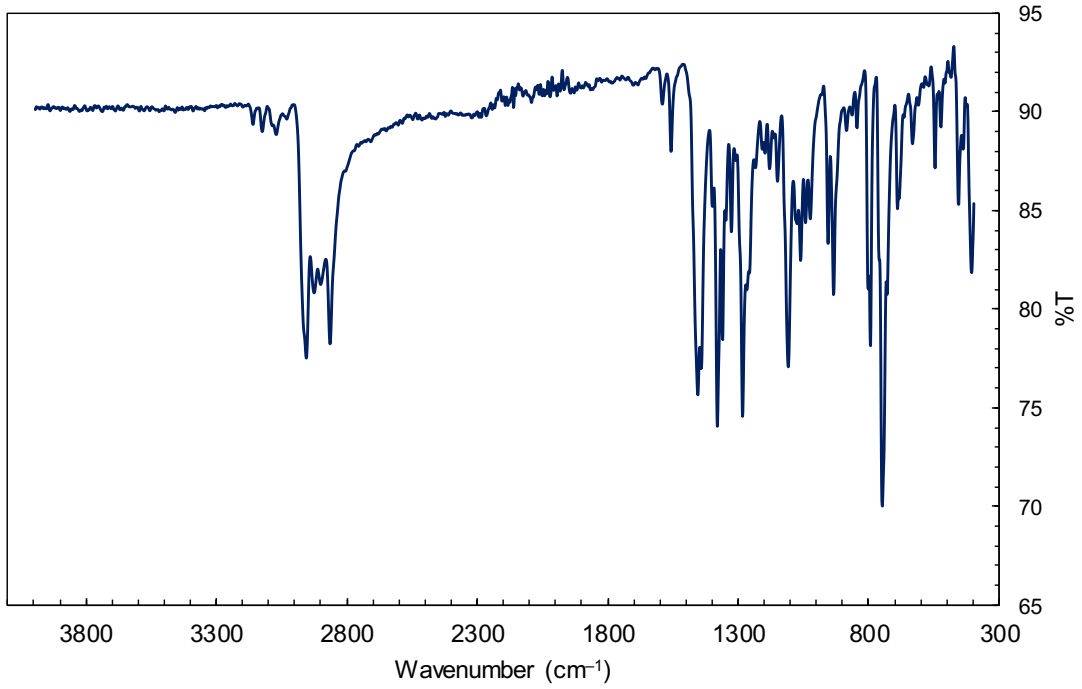

Supplementary Figure 7. FT-IR spectrum of solid **1**.

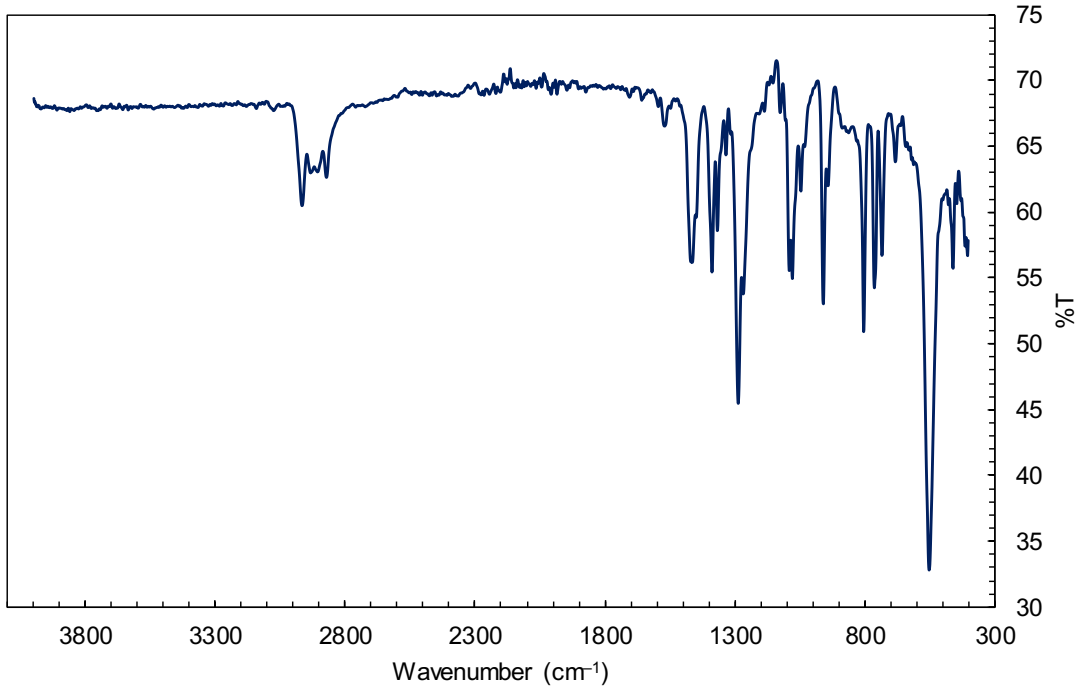

Supplementary Figure 8. FT-IR spectrum of solid **2**.

UV-Vis Spectroscopy

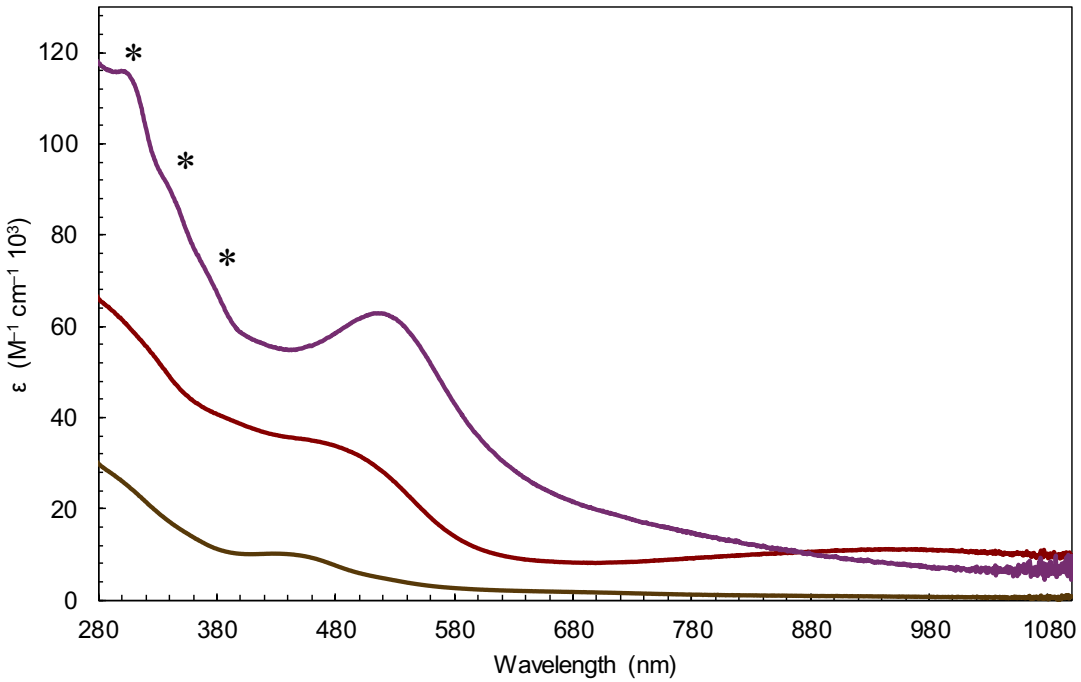

Supplementary Figure 9. UV-Vis spectrum of **1** (brown trace), **2** (red trace), and **3** (purple trace) in the presence of an additional 2 equiv $(C_5(Me)_4SiMe_3)_2Ti$ (purple trace) in *cyc*-C_6H_{12}. * peaks arise from $(C_5(Me)_4SiMe_3)_2Ti$, which is otherwise featureless > 400 nm.

EPR Spectroscopy

X-band CW EPR spectra were collected for clusters **1**–**3** as dilute cyclohexane glasses. The spectrum for even-electron **1** was collected in parallel mode (page S10) and revealed an intense, broad resonance centered on g = 10.1,[80] consistent with an S = 2 ground state as observed for the isoelectronic $TpMoFe_3S_4(PEt_3)_2Cl$ (Tp = tris(pyrazolyl)borate) cluster reported by Holm.[64] Cluster **2** is essentially EPR silent down to 4 K in parallel and perpendicular modes. From this we conclude that **2** remains predominantly dimeric in solution, as the terminal N_2-bound cluster would be odd-electron and thus EPR active.

Cluster **3** is odd-electron and its EPR spectrum (page S11), collected in perpendicular mode, features a strong, broad, pseudo-axial signal with g_{iso} = 1.97 at 4 K, indicating an $S = {}^1/_2$ ground state. The spectrum was collected at 15 K due to signal saturation at low temperatures. No significant population of higher spin excited states was observed at any temperature. The EPR spectrum of the d^1 metalloradical $(C_5(Me)_4SiMe_3)_2Ti^{III}Cl$ collected at the same temperature (page S11) is similar to that observed for **3**, with g_{iso} = 1.96. The g-values for $(C_5(Me)_4SiMe_3)_2Ti^{III}Cl$ as a toluene glass at RT and 130 K have been reported, but the spectrum was not shown[69]. The broadness of the EPR signal shown for **3** and $(C_5(Me)_4SiMe_3)_2Ti^{III}Cl$ indicate what is likely a combination of g-strain and unresolved hyperfine coupling interactions (H-strain), which were accounted for using the appropriate homogenous line broadening parameters.[75]

Given the similarity of their EPR spectra and the chemical shifts of the cyclopentadienyl-derived ^1H resonances for **3** and $(C_5(Me)_4SiMe_3)_2Ti^{III}Cl$, we suggest that the unpaired electron for both resides in an analogous, essentially non-bonding Ti-localized d-orbital.[81] On this basis we describe the electron structure of **3** as a diamagnetic $[MoFe_3S_4][N_2]^-$ fragment bound to an $S = {}^1/_2$ $[(C_5(Me)_4SiMe_3)_2Ti^{3+}]^+$ group (see main text).

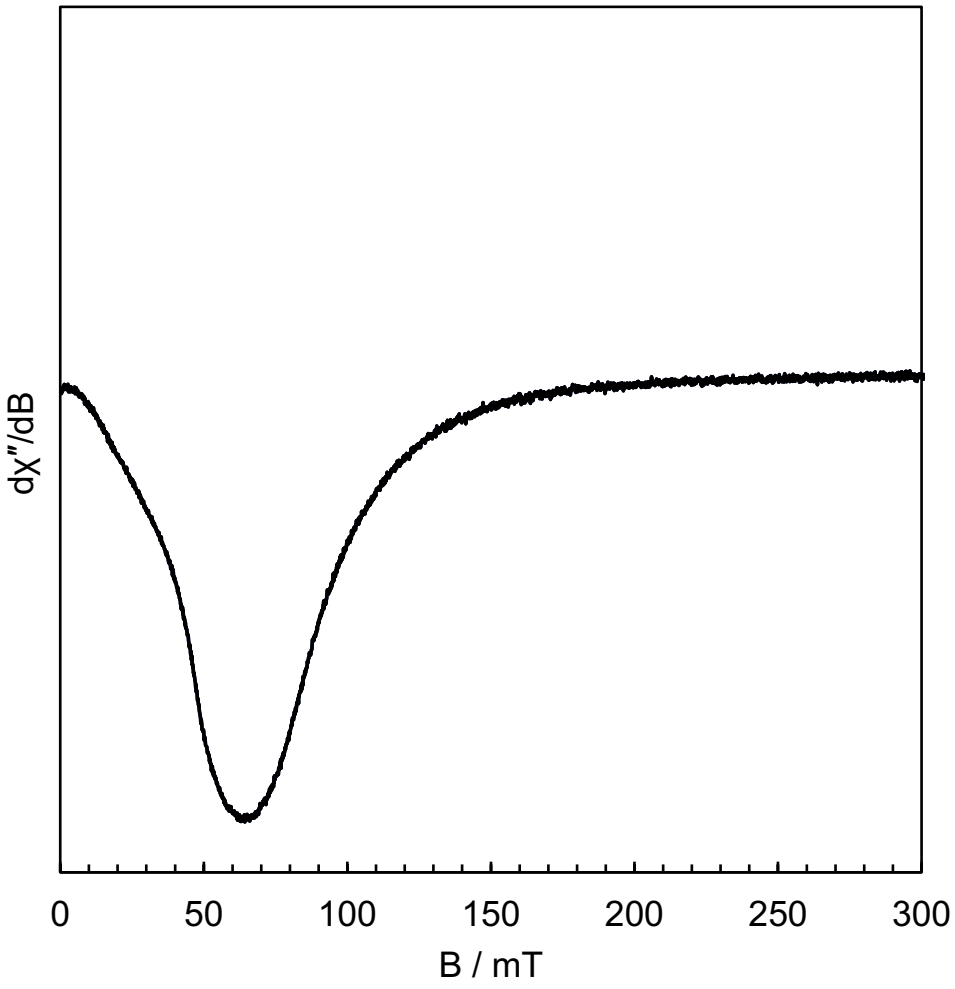

Supplementary Figure 10. CW EPR spectrum of **1** recorded in parallel mode at 9.40 GHz and 1.0 mW power at 10 mM concentration in a *cyc*-C_6H_{12} glass at 4 K.

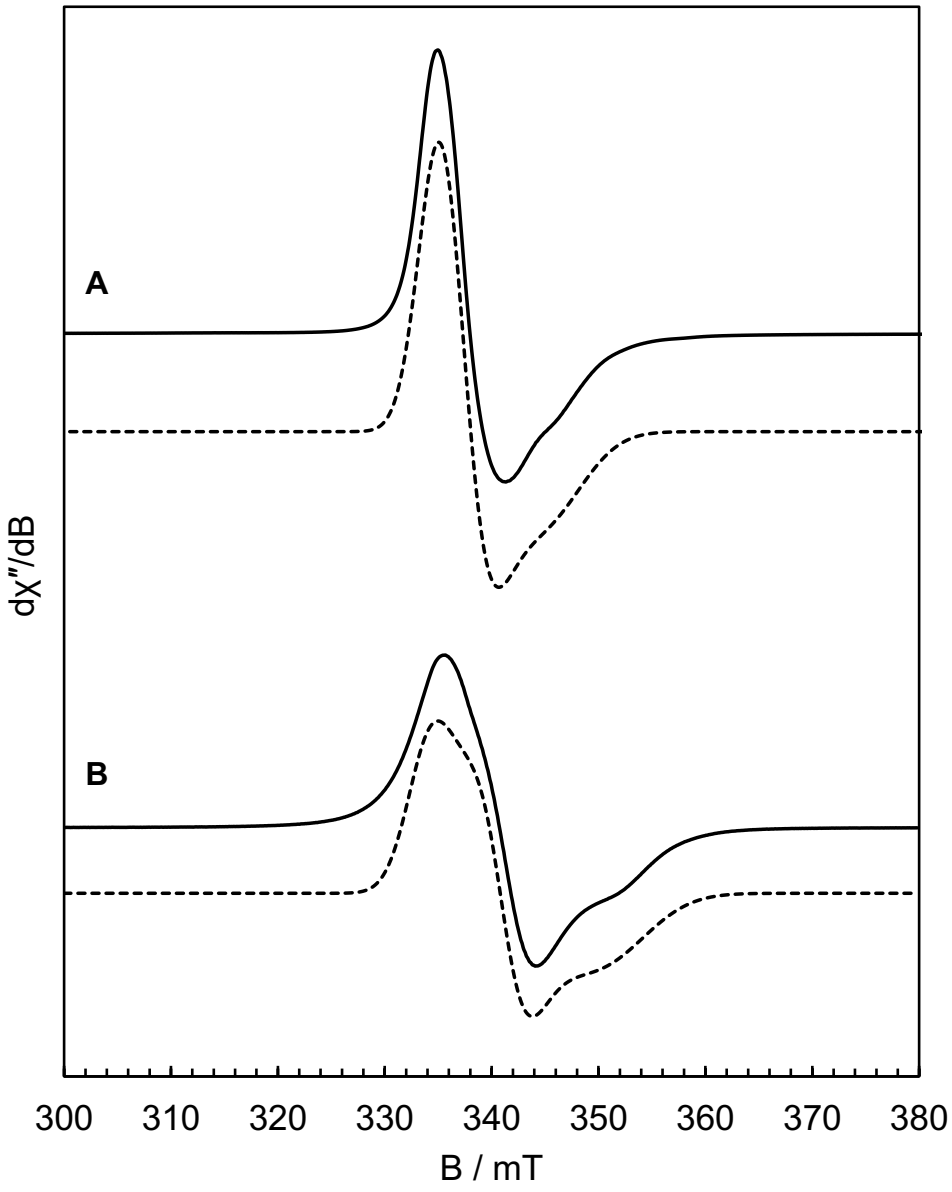

Supplementary Figure 11. CW EPR spectra of (A) **3** and (B) $(C_5(Me)_4SiMe_3)_2Ti^{III}Cl$ recorded in perpendicular mode at 9.37 GHz and (A) 0.25 mW or (B) 0.025 mW power at 1 mM concentration in *cyc*-C_6H_{12} glasses at 15 K. Solid lines are the experimental spectra, dashed lines are the simulations (parameters in Supplementary Table 1).

Supplementary Table 1.

	3			$(C_5(Me)_4SiMe_3)_2Ti$		
g-values	2.00	1.98	1.94	2.00	1.96	1.91
g-strain	0.015	0.20	0.030	0.015	0.20	0.030
H-strain (MHz)	100	100	175	120	90	220
line broadening (MHz)		1			1	

X-ray Crystallography

Supplementary Table 2. Metal-ligand and selected metal-metal bond lengths (Å) obtained from single-crystal XRD studies for clusters **1**–**3**.

		1*	**2**	**3**
Fe(unique)	Cl/N	2.2370(8)	1.811(1)	1.756(1)
	S	2.3123(6)	2.248(1)	2.2613(6)
		2.2830(8)	2.2956(7)	2.2291(8)
		2.3031(5)	2.2517(6)	2.2330(6)
	S (av.)	**2.299(1)**	**2.265(1)**	**2.241(1)**
Fe(IPr)	C	2.011(2)	2.019(2)	1.993(1)
	S	2.2201(7)	2.257(1)	2.2465(7)
		2.2502(6)	2.2332(5)	2.2288(6)
		2.2725(6)	2.2742(6)	2.2293(6)
	S (av.)	**2.248(1)**	**2.244(1)**	**2.235(1)**
Fe(IPr)	C	2.068(1)	2.031(2)	2.004(1)
	S	2.2681(8)	2.257	2.2205(8)
		2.2822(5)	2.2332	2.2520(5)
		2.2794(6)	2.2742	2.2462(6)
	S (av.)	**2.277(1)**	**2.255(1)**	**2.240(1)**
Fe(total)	C (av.)	**2.040(2)**	**2.025(3)**	**1.999(1)**
	S (av.)	**2.275(2)**	**2.254(2)**	**2.239(2)**
Mo	S	2.3207(8)	2.3640(7)	2.3408(6)
		2.3474(6)	2.3315(5)	2.3612(5)
		2.3565(7)	2.337(1)	2.3286(7)
	S (av.)	**2.342(1)**	**2.344(1)**	**2.344(1)**
	Fe	2.7803(5)	2.753(1)	2.7385(7)
		2.6964(6)	2.705(1)	2.7612(8)
		2.7337(6)	2.7493(5)	2.7042(8)
	Fe (av.)	**2.737(1)**	**2.736(1)**	**2.735(1)**
	C (av.)	**2.391(4)**	**2.388(4)**	**2.395(4)**

*The crystal structure of **1** has two unique clusters in the unit cell. The bond metrics for both are very similar and only one set of values is given here; see .cif files for details. Errors for average distances are given as the root sum of the squares of the individual estimated standard deviations.

Note:

Although the Fe–S/C distances for **1**–**3** vary appreciably, the structural metrics for Mo are not statistically different. This is typical; for example, for the reported clusters $[(Tp)MoFe_3S_4(PEt_3)_3]^+$ and $[(Tp)MoFe_3S_4(CN)_3]^{3-}$, one-electron reduction to afford the edge-bridged double cubane $[(Tp)Mo_2Fe_6S_8(PEt_3)_4]$ or $[(Tp)MoFe_3S_4(CN)_3]^{2-}$, respectively, results in only small changes (< 0.02 Å) to the Mo–ligand and Mo–Fe distances.[63,65,82] For these clusters and others the formal oxidation state of Mo is proposed to remain unchanged between different redox levels;[18] we hypothesize likewise. Additional insights into the bonding at Mo await further spectroscopic characterization.

Comparison of Vibrational Data with Other Bridging Fe–N_2–Fe complexes

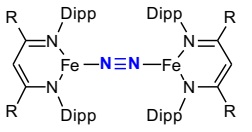

Holland
$2\times Fe^{2+}$ (assuming N_2^{2-} ligand)
Φ(N–N): 1810 cm^{-1} (R = Me); 1778 (R = tBu)
Fe–N (Å): 1.770(4) (R = tBu); 1.779(4) (R = Me)
N–N (Å): 1.182(5) (R = tBu); 1.186(7) (R = Me)
Ref. 44

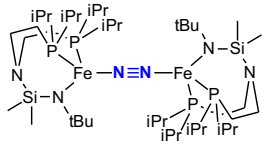

Arnold
$2\times Fe^{1+}$ (assuming N_2 ligand)
ν(N–N): 1760 cm^{-1}
Fe–N (Å): 1.851(1)
N–N (Å): 1.166(1)
Ref. 45

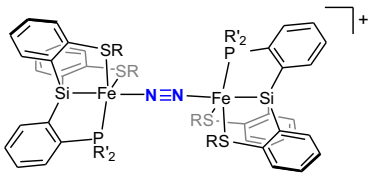

Peters
$1\times Fe^{+}$ $1\times Fe^{2+}$ (assuming N_2 ligand)
Φ(N–N): 1881 cm^{-1} (R = adamantyl; R' = iPr),
1898 (R = adamantyl; R' = Ph),
No structural data
Ref. 40

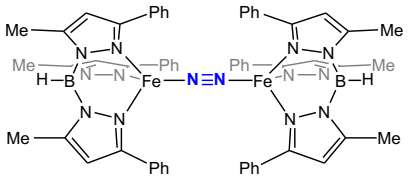

Harman
$2\times Fe^{1+}$ (assuming N_2 ligand)
λ(N–N): 1779 cm^{-1}
Fe–N (Å): 1.790(1)
N–N (Å): 1.181(1)
Ref. 46

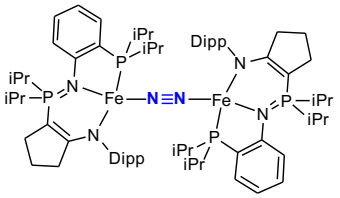

Fryzuk
$2\times Fe^{1+}$ (assuming N_2 ligand)
ι(N–N): 1755 cm^{-1}
Fe–N (Å): 1.800(4), 1.812(4)
N–N (Å): 1.186(6)
Ref. 47

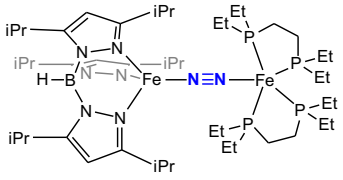

Szymczak
$1\times Fe^{0}$ $1\times Fe^{2+}$ (assuming N_2 ligand)
ϰ(N–N): 1824 cm^{-1}
Fe–N (Å): 1.884(3), 1.887(4)[a]
N–N (Å): 1.177(6), 1.181(5)[a]
Ref. 48

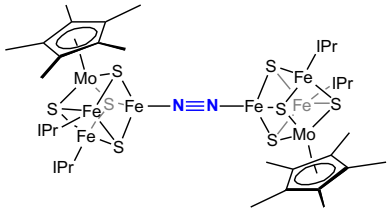

This work
α(N–N): 1834 cm^{-1}
Fe–N (Å): 1.811(2)
N–N (Å): 1.145(3)

Supplementary Figure 12. Data are presented for **2** and Fe–N_2–Fe complexes for which vibrational data have been reported[40,44-48]. Both Fe–N distances are shown for those complexes with crystallographically distinct Fe centers. [a] Only metrics for the Tp-ligated Fe are shown; two molecules of each metal complex are in the unit cell.

Mössbauer Data and Discussion

Mössbauer spectra and associated simulations for clusters **1**–**3** are shown on pages S16–18. For clusters **1** and **3**, excellent three-site simulations were obtained.

For **1**, two simulations of equally good fit were obtained (page S16). Both have in common a subsite with δ = 0.46 mm s^{-1} and $|\Delta E_Q|$ = 2.59 mm s^{-1}. The Mössbauer spectrum of **3** revealed solid samples of this cluster to be contaminated with small amounts of solid **2** (13.7% total Fe content), signals for which were subtracted prior to simulation (page S18). For **3**, only one reasonable three-site simulation was found (page S18). For **1** and **3**, these simulations were used to calculate δ_{av} (see main text). At this stage, we are unable to unambiguously assign any one quadrupole doublet to a specific Fe subsite for **1** or **3**, but we can conclude that the isomer shift of each Fe site in **1** is greater than the isomer shift of each Fe site in **3**, which is consistent with increased covalency throughout the cluster in **3** compared with **1**.

For the Mössbauer spectrum of **2**, we first obtained a qualitative simulation using curve-fitting. This was done by fitting the spectrum to three quadrupole doublets with unrestricted relative areas. The simulation shown in the main text was so obtained using the parameters in Supplementary Table 3.

Supplementary Table 3. Fitting parameters for the 80 K Mössbauer spectrum of **2**.

Site	δ (mm s^{-1})	$\lvert\Delta E_Q\rvert$ (mm s^{-1})	Γ (mm s^{-1})	rel. area
1	0.498	1.262	0.37	0.468
2	0.473	1.914	0.33	0.254
3	0.455	2.237	0.31	0.322

δ_{av} was obtained by taking the weighted average of the above δ values; *i.e.*:

$$\delta_{av} = \frac{\sum_i (\delta_i \times (\text{rel. A})_i}{\sum_i (\text{rel. A})_i}$$

The Mössbauer spectrum of **2** was also simulated using a three-site model, for which each site has the same relative area (page S17). Although a reasonable fit is obtained, the quadrupole doublet for one subsite is unusually broad (Γ = 0.54 mm s^{-1}). We are at this stage unable to account for this phenomenon, which could have multiple origins; a more detailed Mössbauer study will be forthcoming.

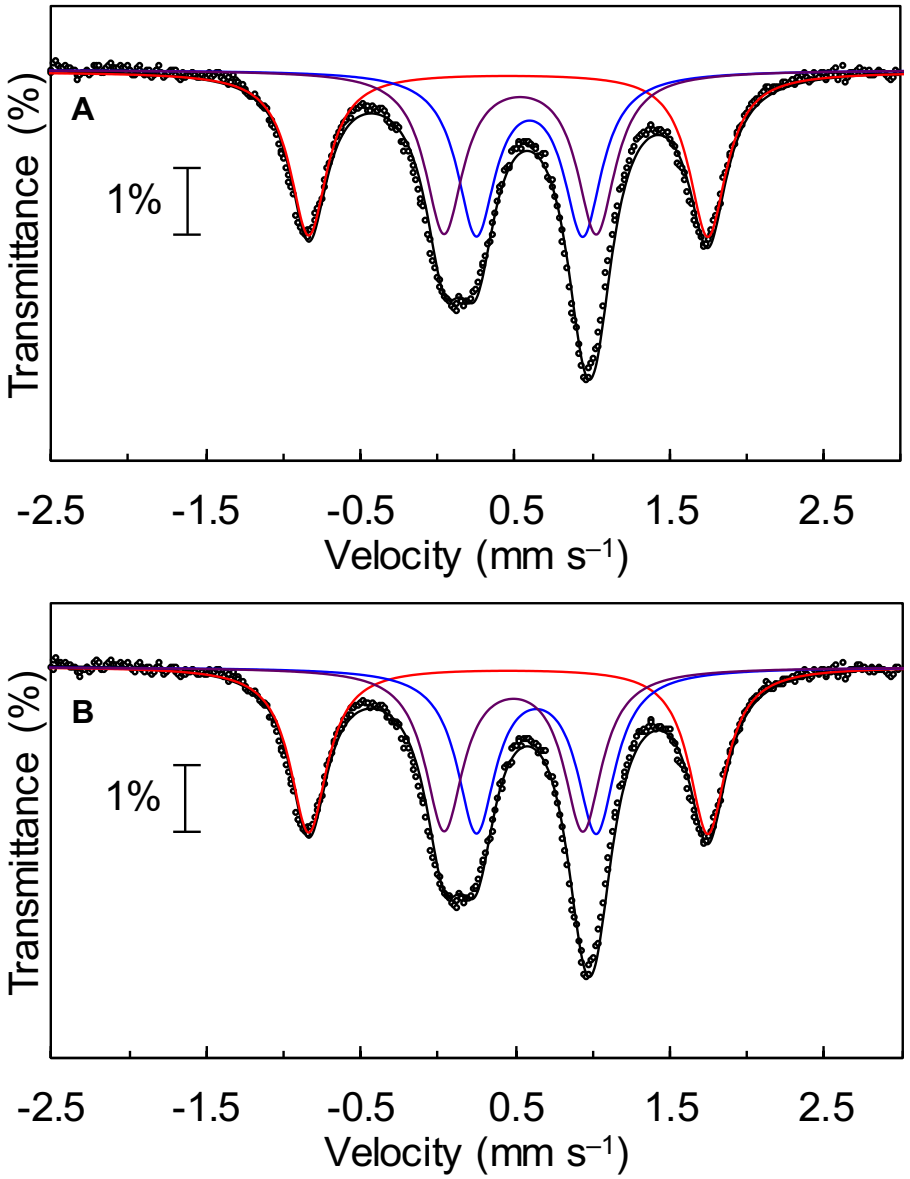

Supplementary Figure 13. Two statistically indistinguishable simulations of the zero-field ^{57}Fe Mössbauer spectra (80 K) of solid **1**. Black circles = experimental data; total simulation = black line; colored lines = individual site simulations (parameters below, values in mm s^{-1}).

Supplementary Table 4. Fitting parameters for the 80 K Mössbauer spectrum of **1**.

	A				**B**			
Site	δ (mm s^{-1})	$\lvert\Delta E_Q\rvert$ (mm s^{-1})	Γ (mm s^{-1})	Rel. area	δ (mm s^{-1})	$\lvert\Delta E_Q\rvert$ (mm s^{-1})	Γ (mm s^{-1})	Rel. area
red	0.456	2.585	0.29	1	0.456	2.585	0.29	1
blue	0.594	0.691	0.30	1	0.638	0.777	0.30	1
purple	0.533	0.986	0.30	1	0.490	0.899	0.30	1

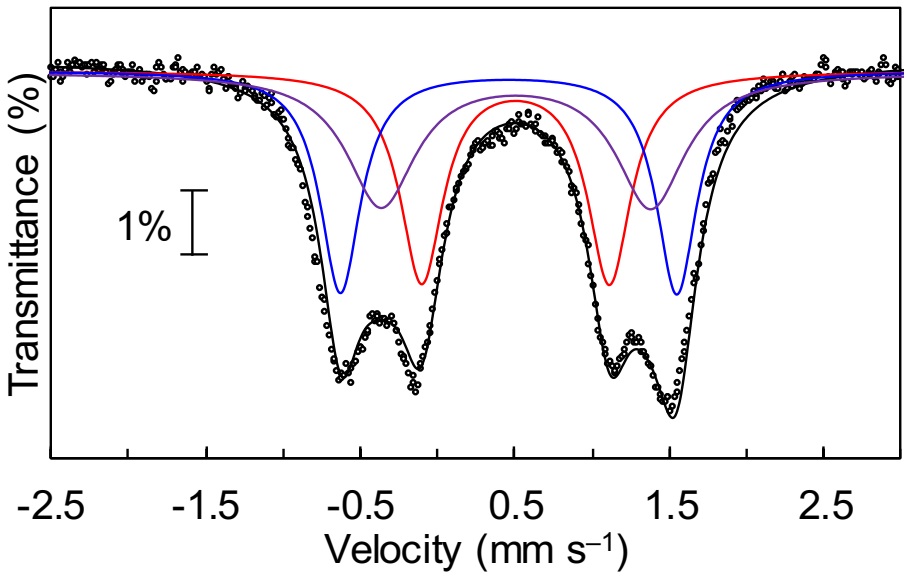

Supplementary Figure 14. Zero-field ^{57}Fe Mössbauer spectra (80 K) of solid **2** using a three-site model for the simulations (see discussion above). Black circles = experimental data; total simulation = black line; colored lines = individual site simulations (parameters below, values in mm s^{-1}).

Supplementary Table 5. Fitting parameters for the 80 K Mössbauer spectrum of **2** using a three-site model.

Site	δ (mm s^{-1})	$\lvert\Delta E_Q\rvert$ (mm s^{-1})	Γ (mm s^{-1})	rel. area
red	0.504	1.216	0.34	1
blue	0.459	2.179	0.32	1
purple	0.506	1.747	0.54	1

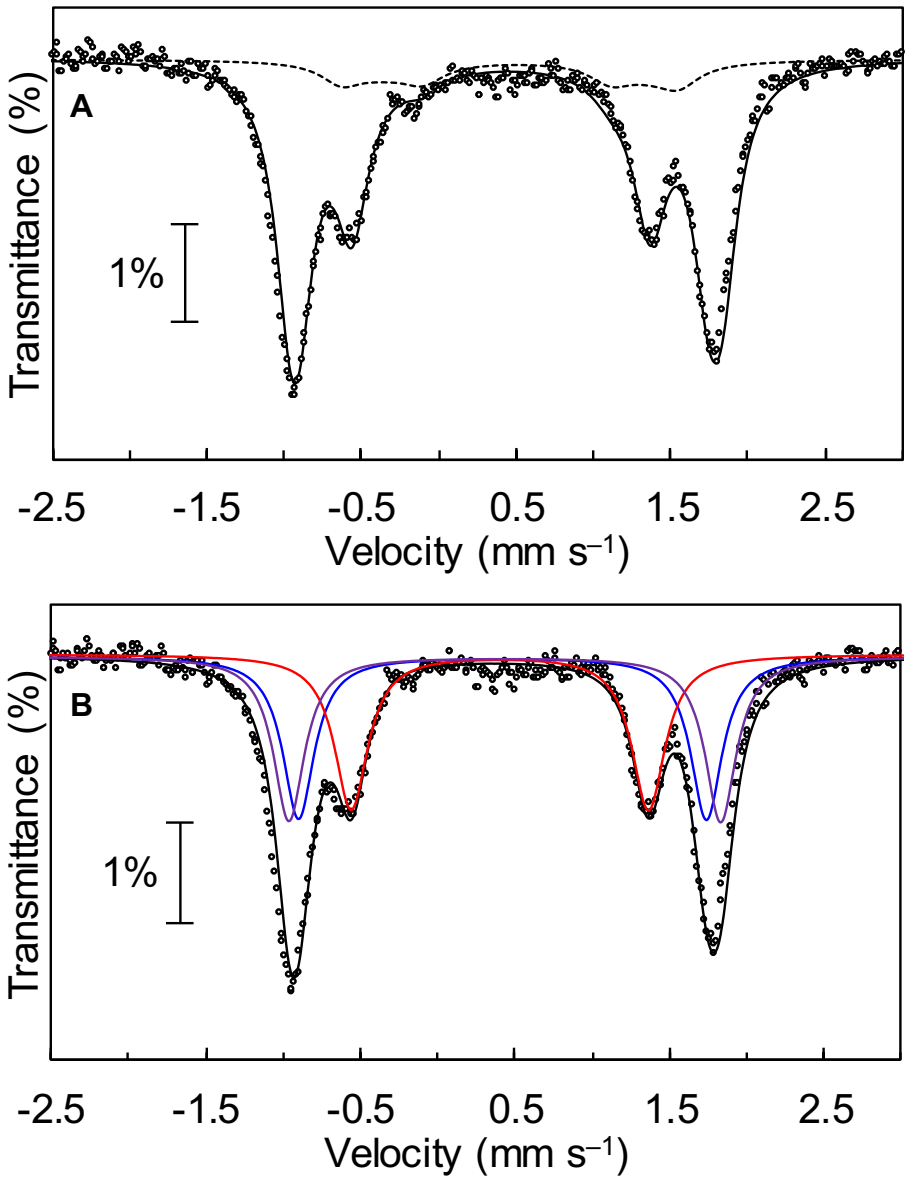

Supplementary Figure 15. Zero-field ^{57}Fe Mössbauer spectra (80 K) of solid **3** (A) as recorded and (B) after subtraction of the signal due to **2**. Black circles = experimental data; total simulation = black line; dashed line for (A) = simulation of **2** (13.7% of the total Fe content; colored lines = individual site simulations (parameters below, values in mm s^{-1}).

Supplementary Table 6. Fitting parameters for the 80 K Mössbauer spectrum of **3**.

Site	δ (mm s^{-1})	$\lvert\Delta E_Q\rvert$ (mm s^{-1})	Γ (mm s^{-1})	rel. area
red	0.401	1.926	0.26	1
blue	0.419	2.642	0.26	1
purple	0.433	2.797	0.24	1

Supplementary References

80. Hendrich, M. P. & Debrunner, P. G. Integer-spin electron-paramagnetic resonance of iron proteins. *Biophys. J.* **56**, 489-506 (1989).

81. Lukens, W. W., Smith, M. R. & Andersen, R. A. A π-donor spectrochemical series for X in $(Me_5C_5)_2TiX$, and β-agostic interactions in X=Et and N(Me)Ph. *J. Am. Chem. Soc.* **118**, 1719-1728 (1996).

82. Pesavento, R. P., Berlinguette, C. P. & Holm, R. H. Stabilization of reduced molybdenum-iron-sulfur single- and double-cubane clusters by cyanide ligation. *Inorg. Chem.* **46**, 510-516 (2007).